Dynamics of Solar and Stellar Convection Zones and Atmospheres
Proceedings IAU Symposium No. 365, 2024
A. V. Getling & L. L. Kitchatinov, eds.
doi:10.1017/S1743921324000164

A Frequency-Dependent Method for Measuring the Sun's Interior Meridional Circulation

Ruizhu Chen and Junwei Zhao

W. W. Hansen Experimental Physics Laboratory, Stanford University, Stanford, CA, USA
email: rzchen@stanford.edu

Abstract. The Sun's meridional circulation is a crucial component for understanding the Sun's dynamo and its interior dynamics. However, the determination of meridional circulation is affected by a systematic center-to-limb (CtoL) effect, which introduces systematic errors 5–10 times stronger than the meridional-flow-induced travel-time shifts in deep-flow measurements. Recently, it was found that the CtoL effect has a significant acoustic-frequency dependence, while flow-induced travel-time shifts show little frequency dependence (Chen & Zhao 2018). This discovery forms the basis for designing a new method to remove the CtoL effect. We therefore propose a frequency-dependent approach to measure the CtoL effect and the flow-induced signals in the Fourier domain. In this work, we present this new method and compare time–distance measurements in different frequency bands with those obtained by previous time-domain methods. The results demonstrate consistency with conventional time-domain fitting methods in the dominant frequency range, promising the potential for conducting meridional flow inversion across a broader frequency spectrum.

Keywords. Sun: helioseismology, Sun: interior, Sun: oscillations

1. Introduction

The Sun's meridional circulation is a critical element in understanding the Sun's dynamo and internal dynamics. While direct observation of solar deep interior flows is not possible, time-distance helioseismology offers a way to infer these flows by measuring the acoustic travel times of p-mode waves traveling inside the Sun (Duvall *et al.* 1993). However, it was found that these time–distance measurements are complicated by a systematic center-to-limb variation (Zhao *et al.* 2012). This systematic effect, known as the Center-to-Limb (CtoL) effect, has been consistently observed across multiple instruments and by different authors (Zhao *et al.* 2013; Kholikov *et al.* 2014; Jackiewicz *et al.* 2015; Liang & Chou 2015b; Rajaguru & Antia 2015; Liang *et al.* 2017; Chen & Zhao 2017; Gizon *et al.* 2020), yet its underlying cause remains elusive. Of particular concern is the fact that the CtoL effect can be an order of magnitude larger than the travel-time shifts induced by flows for deep regions, significantly impacting the accurate inference of the Sun's meridional circulation. Addressing and removing this effect remains as a major challenge in the field of solar meridional flow measurements.

Recent findings by Chen & Zhao (2018) have shed light on the CtoL effect measured in time-distance helioseismology, revealing a strong acoustic-frequency dependence that

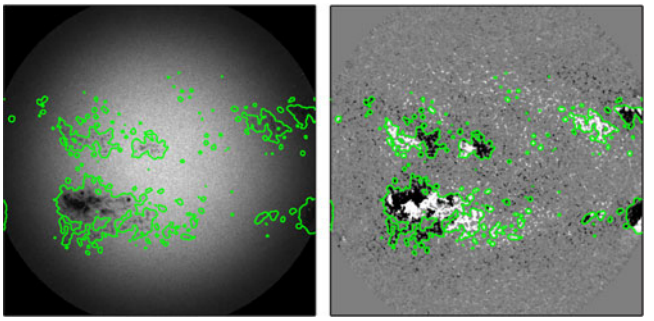

Figure 1. (Left) Daily acoustic power map of 2012 July 8, with green contours of 10 Gauss threshold on the daily-averaged magnetograms, inside which Doppler data are not used in our time–distance measurements. (Right) Line-of-sight magnetic field image captured on the same date, with identical contours overlaid.

reverses sign at a specific frequency. This unique frequency dependence, in contrast to the relatively frequency-independent nature of flow-caused travel-time shifts, not only provides potential insights into the origin of the systematic effect but also suggests a novel approach to disentangling the CtoL effect from meridional flow signals in the frequency domain. Traditional time-domain fitting of travel-time shifts primarily captures signals within dominant frequency ranges, overlooking the frequency-dependent differences between the CtoL effect and flow-induced travel-time shifts. Exploiting information across a wider frequency range holds the promise of extracting richer details from the observed signals.

In this study, we extend the investigation initiated by Chen & Zhao (2018) by conducting frequency-dependent measurements of both the CtoL effect and meridional-flow-induced travel-time shifts. We compare the meridional-flow travel-time shift signals measured across multiple frequency bands and in the time domain. The paper is organized as follows: Section 2 introduces the data preparation, Section 3 outlines the methodology and presents measurements, and Section 4 discusses our findings.

2. Data Preparation

We utilize HMI full-disk Doppler observations, covering the period from May 1, 2010, to April 30, 2021, a total of 11 years' worth of data. We first downsample full-disk images to 1024×1024 pixels, track them using the Snodgrass rotation rate at the disk center, and project them onto Postel's coordinates, with the disk center as the image center. Subsequently, we further downsample the tracked images to 425×425 pixels, resulting in a spatial resolution of $0.^{\circ}36$ pixel^{-1} (where 1° represents 1 heliographic degree) at the disk center. For the analysis, we employ running-difference data to eliminate solar convection, and no additional filtering is applied.

The influence of surface magnetic effects on travel time anomalies becomes apparent when measurements are taken in magtnetic regions (Gizon et al. 2009; Liang & Chou 2015a). To address this, we apply a threshold of 10 Gauss to mask magnetic regions on the daily-averaged and Gaussian-smoothed line-of-sight magnetic field maps. It's noteworthy that despite the seemingly small value of 10 Gauss, this threshold is considered appropriate as magnetic fields are substantially averaged. Figure 1 provides an illustrative example, depicting a daily acoustic oscillation power map along a magnetogram map, with the applied mask overlaid for reference.

https://doi.org/10.1017/S1743921324000164 Published online by Cambridge University Press

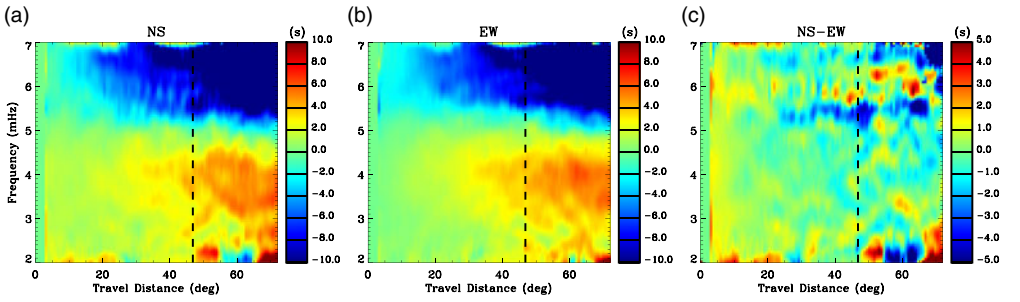

Figure 2. (a) Travel-time shifts $\delta\tau_{NS}$ measured along the NS direction at 32.°4 latitude on the central meridian, displayed as functions of travel distance and frequency. Black-dashed line indicates the approximate travel distance for waves passing the BCZ, beyond which the data are typically not robust enough for inversion and are generally not used in inversions. (b) Same but for $\delta\tau_{EW}$ measured along the EW direction at 32.°4 longitude on the Equator. (c) $\delta\tau_{NS} - \delta\tau_{EW}$, illustrating the meridional-flow-caused travel-time shifts.

3. Frequency-Dependent Measurement Approach

In previous time-distance helioseismic measurements, travel times were conventionally fitted from the cross-covariance functions in the time domain, often using techniques such as Gabor-wavelet fitting. The travel-time shifts used for flow inversion were then determined by taking the differences between the travel times of waves traveling in opposite directions. In our current study, we adopt the methodology developed by Chen & Zhao (2018) to derive frequency-dependent travel-time shifts in the Fourier domain. This involves calculating the relative phase differences between the positive- and negative-time-lag segments of the cross-covariance function, and then convert the phase differences to travel-time shifts. We have enhanced the method by imcoporating a refined whitening profile and windowing functions utilized in the calculation (refer to Section 2.3 of Chen & Zhao (2018)). These empirical profiles used are now tailored as functions of both disk location and travel distance, determined from 11 years of data. We have also modified the phase averaging strategy. Consequently, the current measurements are less noisy with little aliasing effect..

3.1. *Measurements of the CtoL Effect and Meridional Flow-Induced Travel-Time Shifts*

We proceed to conduct time-distance measurements in the equatorial region along the East-West (EW) direction and in the central meridian regions along the North-South (NS) direction. All measurements are performed between pairs of arcs positioned along the disk-radial direction, and the focus points of the arc pairs are situated within a narrow sector spanning $\pm 10°$ around the disk center (refer to the illustration of the EW scheme in Figure 1 of Chen & Zhao (2018)). The resulting series of cross-covariance functions, measured as a function of travel distance and disk location, are utilized to calculate the frequency-dependent travel-time shifts. The outcomes for NS and EW measurements, along with their difference, are illustrated in Figure 2.

The frequency-dependent travel-time shifts measured along both the NS and EW directions exhibit significant frequency dependence. The EW results presented in Figure 2(b) have already removed its zonal flow components by removing its symmetric component around disk center. Following this adjustment, the remaining EW signals are often considered as a proxy for the CtoL effect. By subtracting this CtoL proxy from the NS results, the residual signals in Figure 2(c) are considered as the meridional-flow-induced travel-time shifts.

https://doi.org/10.1017/S1743921324000164 Published online by Cambridge University Press

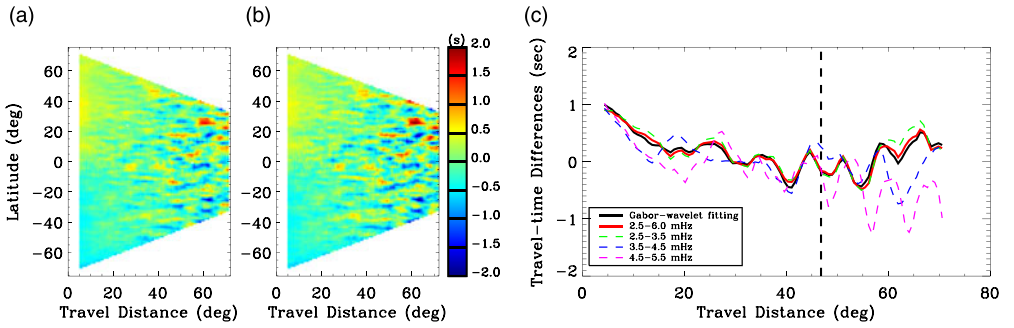

Figure 3. (a) Time-domain measurement of $\delta\tau_{NS} - \delta\tau_{EW}$ by Gabor-wavelet fitting. (b) Fourier-domain measurement of $\delta\tau_{NS} - \delta\tau_{EW}$ in 2.5-6mHz (power-weighted average). (c) Comparison of the time-domain and Fourier-domain measurements of $\delta\tau_{NS} - \delta\tau_{EW}$ for 10° - 30° latitudes. The black-dashed line indicates the approximate travel distance for waves passing the BCZ.

The flow-induced signal exhibits little frequency dependence for frequencies below 5 mHz and for travel distances smaller than the black-dashed line, representing the approximate travel distance for waves passing the base of the convection zone (BCZ). Typically, only measurements shallower than this are considered robust and will be utilized in inversions. Within this range, the results at different frequencies appear consistent, promising the potential of getting consistent results through inverting measurements of various frequency bands.

However, the measurements become considerably noisier beyond approximately 5 mHz or beyond about 40°travel distance. Notably, it still displays aliasing artifacts, appearing as alternating bands of positive and negative phases in the higher-frequency bands, despite our efforts to mitigate these artifacts through improved methods. Completely eliminating these artifacts proves challenging due to the weak oscillation signals in the high-frequency range. Nevertheless, it is essential to acknowledge that these artifacts are most severe for high frequencies and large distances, and the low-frequency and small-travel-distance results, on the other hand, remain useful despite these challenges.

3.2. *Comparative Analysis with Time-Domain Method*

In the range below about 5 mHz and for small travel distances, where the results exhibit robustness, we proceed to conduct a comparison of the travel-time shift curves in multiple frequency bands with those obtained through conventional time-domain fitting methods.

Figure 3 presents the time-domain result of $\delta\tau_{NS} - \delta\tau_{EW}$, along with the wide-band (2.5-6 mHz) power-weighted-average result, indicating a noticeable similarity between the two. Their values in the 10° - 30° range are further compared in Figure 3(c), along with those from 1-mHz narrow-band results around 3, 4, and 5 mHz. The curves for the wide-band and dominant frequency band (2.5-3.5 mHz) are almost identical due to the prominent dominance of oscillation power around the 3.3 mHz peak. Both of them are also nearly identical to the time-domain results, indicating consistency with the time-domain fitting method. The curve for 3.5-4.5 mHz remains consistent but exhibits some noise. Results for 4.5-5.5 mHz become noisier and show slight deviations, yet these deviations are not significant compared to their error level (~ 0.5 seconds).

https://doi.org/10.1017/S1743921324000164 Published online by Cambridge University Press

4. Discussion

We have devised a new procedure for conducting frequency-dependent measurements of the meridional-flow-induced travel-time shifts and the associated CtoL effects. In the dominant frequency range, the method yields nearly identical results when compared to time-domain fitting. Yet its advantage lies in the potential for conducting flow inversions across a broader frequency spectrum, expanding the scope of our understanding across multiple frequency bands.

Ideally, the inversion of meridional flow using different frequency bands should yield consistent results since the interior flow remains the same regardless of acoustic wave frequencies. This consistency serves as a criterion to assess whether systematic effects are appropriately removed, whether inversions are conducted effectively, and whether the results are reliable. A recent study by Rajaguru & Antia (2020) also conducts frequency-dependent meridional flow measurements by applying frequency filters before fitting travel times. Their findings reveal a noticeable difference, showing a single-cell circulation profile in 3 mHz and a double-cell profile in 4 mHz, suggesting unresolved challenges in the measurement process.

In our results, we have also noted variations in travel-time shifts at higher frequencies. However, understanding how these differences translate into inverted flow profiles requires further investigation, as the sensitivity of travel-time shifts could also vary with frequency. In future studies, we plan to perform meridional flow inversions using frequency-dependent sensitivity kernels (Hartlep & Zhao 2021). Additionally, we acknowledge the presence of remaining artifacts in the high-frequency range above 5.0 mHz, which could potentially be further addressed in future works.

Acknowledgements. *SDO* is a NASA mission, and HMI project is supported by NASA contract NAS5-02139 to Stanford University. R.C. and J.Z. are partly supported by NASA DRIVE Center COFFIES grant 80NSSC22M0162.

References

Chen, R., & Zhao, J. 2017, *Astrophys. J.*, 849, 144
Chen, R., & Zhao, J. 2018, *Astrophys. J.*, 853, 161.
Duvall, T. L., Jr., Jefferies, S. M., Harvey, J. W., & Pomerantz, M. A. 1993, *Nature*, 362, 430
Gizon, L., Cameron, R. H., Pourabdian, M., *et al.* 2020, *Science*, 368, 1469.
Gizon, L., Schunker, H., Baldner, C. S., et al. 2009, *Space Sci. Rev.*, 144, 249.
Hartlep, T., & Zhao, J. 2021, *Astrophys. J.*, 909, 66.
Jackiewicz, J., Serebryanskiy, A., & Kholikov, S. 2015, *Astrophys. J.*, 805, 133
Kholikov, S., Serebryanskiy, A., & Jackiewicz, J. 2014, *Astrophys. J.*, 784, 145
Liang, Z.-C., Birch, A. C., Duvall, T. L., Jr., Gizon, L., & Schou, J. 2017, *A&A*, 601, A46
Liang, Z.-C., & Chou, D.-Y. 2015a, *Astrophys. J.*, 805, 165
Liang, Z.-C., & Chou, D.-Y. 2015b, *Astrophys. J.*, 809, 150
Rajaguru, S. P., & Antia, H. M. 2015, *Astrophys. J.*, 813, 114
Rajaguru, S. P. & Antia, H. M. 2020, *Dynamics of the Sun and Stars; Honoring the Life and Work of Michael J. Thompson*, 57, 107.
Zhao, J., Bogart, R. S., Kosovichev, A. G., Duvall, T. L., Jr., Hartlep, T. 2013, *Astrophys. J. Letters*, 774, L29
Zhao, J., Nagashima, K., Bogart, R. S., Kosovichev, A. G., Duvall, T. L., Jr. 2012, *Astrophys. J. Letters*, 749, L5